

# UC Irvine

## UC Irvine Previously Published Works

### Title

Electrochemical Quantification of Glycated and Non-glycated Human Serum Albumin in Synthetic Urine

### Permalink

<https://escholarship.org/uc/item/9dx6x75b>

### Journal

ACS Applied Materials & Interfaces, 11(5)

### ISSN

1944-8244

### Authors

Attar, Aisha M  
Richardson, Mark B  
Speciale, Gaetano  
et al.

### Publication Date

2019-02-06

### DOI

10.1021/acsami.8b16071

Peer reviewed



Published in final edited form as:

*ACS Appl Mater Interfaces*. 2019 February 06; 11(5): 4757–4765. doi:10.1021/acsami.8b16071.

## Electrochemical quantification of glycated and non-glycated human serum albumin in synthetic urine

Aisha M. Attar<sup>†</sup>, Mark B. Richardson<sup>†</sup>, Gaetano Speciale<sup>†</sup>, Sudipta Majumdar<sup>†</sup>, Rebekah P. Dyer<sup>‡</sup>, Emily C. Sanders<sup>†</sup>, Reginald M. Penner<sup>\*,†</sup>, and Gregory A. Weiss<sup>\*,†,‡</sup>

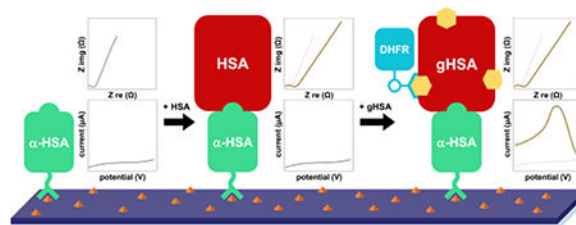
<sup>†</sup> Department of Chemistry, University of California, Irvine, CA 92697-2015 USA

<sup>‡</sup> Department of Molecular Biology & Biochemistry, University of California, Irvine CA 92697 USA

### Abstract

A polymer-based electrode capable of specific detection of human serum albumin, and its glycated derivatives, is described. The sensor is constructed from a glass microscope slide coated with a synthesized, polythiophene film bearing a protected, iminodiacetic acid motif. The electrode surface is then further elaborated to a functional biosensor through deprotection of the iminodiacetic acid, followed by metal-affinity immobilization of a specific and high-affinity, albumin ligand. Albumin was then quantified in buffer and synthetic urine via electrochemical impedance spectroscopy. Glycated albumin was next bound to a boronic acid-modified, single-cysteine dihydrofolate reductase variant to quantify glycation ratios by square-wave voltammetry. The platform offers high sensitivity, specificity, and reproducibility in an inexpensive arrangement. The detection limits exceed the requirements for intermediate-term glycemic control monitoring in diabetes patients at 5 and 1 nM for albumin and its glycated forms, respectively.

### Graphical Abstract



\*Corresponding Authors: gweiss@uci.edu Phone: 949-824-5566. rmpenner@uci.edu Phone: 949-824-8572.

The authors declare the following competing financial interest(s): The biosensor described here has been licensed to PhageTech, a company co-founded by Drs. Penner and Weiss. PhageTech is developing products related to the research described here. The terms of this arrangement have been reviewed and approved by the University of California, Irvine in accordance with its conflict of interest policies.

Associated Content:

\* Supporting Information

The Supporting Information is available free of charge on the ACS Publications website at DOI: 10.1021/acsami.xrefXXXXXXXX. The supporting information file contains a list of additional recent HSA sensing literature, SEM and AFM images of the PEDOT-pIDA surface, an assessment of five different metal ions for affinity-immobilization, EIS signal-to-noise measurements, <sup>1</sup>H, <sup>13</sup>C NMR and IR spectra for EDOT-pIDA and its synthetic intermediates, methods for the cloning and purification of  $\alpha$ HSA and N37C/C85A/C152S DHFR, and enzymatic activity assays. (PDF)

## Keywords

human serum albumin; glycated albumin; polythiophene; iminodiacetic acid; boronic acid; dihydrofolate reductase; biosensor

## Introduction

Human serum albumin (HSA) is a useful disease biomarker.<sup>1</sup> In healthy adults, the concentration of HSA in blood is 500–800  $\mu\text{M}$ , and  $<0.3 \mu\text{M}$  in urine.<sup>2,3</sup> Elevated urine HSA concentrations (0.3–3  $\mu\text{M}$ ) indicate renal failure or kidney damage, often associated with hypertension and diabetes mellitus (DM).<sup>4–6</sup> Glycation is the non-enzymatic, post-translational addition of carbohydrates to proteins.<sup>7–9</sup> Glycated HSA (gHSA) is typically modified at the free amines of its *N*-terminus and lysine sidechains.<sup>10,11</sup> Healthy adults exhibit blood serum gHSA levels of 11–16% (as a proportion of total HSA), whereas DM patients present with levels of 20–30%.<sup>2</sup> Thus, gHSA has emerged as an important, intermediate-term glycemic control marker, and can report average blood glucose concentrations over the 2–3 week lifetime of HSA in blood.<sup>12–15</sup>

Standard methods for HSA quantification are either antibody-based (immunonephelometry, immunoturbidity, enzyme-linked immunosorbent assays, immunoelectrophoresis, and radio- and chemiluminescent immunoassays), or employ HAS-specific fluorogenic dyes.<sup>16–22</sup> gHSA detection and quantification typically involves automated analyzers, such as the Lucica® GA-L (Asahi-Kasei Pharma, Japan). This and similar instruments use proteolytic digestion and a colorimetric assay to detect glycated amino acids.<sup>23–26</sup> Extensive innovation has been reported over the past decade in the detection of HSA and gHSA, and improved luminescence methods<sup>27–35</sup> dominate the literature (Figure S1). Advanced materials could offer flexibility and tenability, which is difficult to achieve with conventional luminescence-based assays.

We report a modified poly-ethylenedioxythiophene (PEDOT) electrode capable of detecting and quantifying both HSA and gHSA in a single sample. The high synthetic tractability of this organic polymer has facilitated the creation of a diverse repertoire of functional derivatives for sensing applications.<sup>36–40</sup> The device reported here employs a C-terminal, His<sub>6</sub>-tagged GFP construct immobilized on a PEDOT surface via formation of a ternary complex with copper(II), and an iminodiacetic acid (IDA) motif present within the PEDOT film (Figure 1a).<sup>41</sup> Previously, we described electrodeposited phage-PEDOT films for biosensing.<sup>42,43</sup> Here, the phage-derived peptide is fused to GFP (aa sequence of DCPIYCEDGYCLRKCVDLYR)<sup>42</sup> which binds with equal apparent affinities for both HSA and gHSA. This affinity reagent (hereinafter referred to as  $\alpha\text{HSA}$ ) was acquired via recombinant protein expression. The PEDOT-Cu- $\alpha\text{HSA}$ -HSA quaternary complex generates distinctive electrochemical impedance spectra (EIS), allowing total HSA+gHSA concentrations to be quantified (Figure 1b).

The HSA/gHSA ratio was determined utilizing a boronate-tagged, engineered variant of the redox enzyme, dihydrofolate reductase (DHFR), as an electrochemical reporter (Figure 2). The boronate affinity-tag associates selectively with the carbohydrate components of gHSA.

<sup>16,44</sup> The gHSA-immobilized DHFR reporter catalyzes a  $2e^-$  reduction of dihydrofolic acid to tetrahydrofolic acid with NADPH as the reducing agent. Under an applied potential, the tetrahydrofolic acid is oxidized, and its electrons are passed to the PEDOT electrode for detection (Figure 2b). Thus, an exquisitely sensitive, switchable-mode sensor capable of dual quantification of total HSA, and gHSA ratios is realized.

## Results and Discussion

The PEDOT electrode was constructed from a 95:5 mixture of EDOT and an EDOT derivative bearing an anhydride-protected IDA motif (EDOT-pIDA). A surprisingly stable anhydride, the EDOT-pIDA monomer was synthesized in one step from existing literature compounds (Scheme 1). The mixture was copolymerized onto a glass surface pretreated with nitrocellulose adhesive (collodion) and  $\text{Fe}(\text{ClO}_4)_3$  as the requisite polymerization oxidant. Protection of IDA as its anhydride prevents chelation of Fe(III) during this step. After thorough washing of the polymer surface, the essential IDA motif was liberated via base-catalyzed hydrolysis of the anhydride to yield PEDOT-IDA. Six rounds of iterative copolymerization with 95:5 EDOT:EDOT-pIDA mixtures resulted in optimal device performance (Figures S2–S4).<sup>45</sup> Interrogation of the PEDOT-pIDA electrode by SEM and AFM revealed a moderately rough surface, and therefore a large effective sensing surface area (Figures S5 and S6). The ternary PEDOT-Cu- $\alpha$ HSA complex formed spontaneously at ambient temperatures after sequential treatment with aqueous  $\text{CuSO}_4$ , then buffered  $\alpha$ HSA solution.

To apply this material to HSA sensing, EIS measurements were visualized as Nyquist plots (Figure 3a,b). Frequency-dependent impedance differences ( $Z_{re}$  and  $Z_{im}$ ) were well-correlated with analyte concentrations (Figure 3c,d,e,f).  $Z_{total}$  increased with HSA concentration at low frequencies (5 to 50 Hz), but over a wider range for gHSA (5 to 10,000 Hz). For both analytes, the low frequency range of 5 to 50 Hz provided the most significant increases in  $Z_{total}$ . The signal-to-noise ratios for  $Z_{re}$  and  $Z_{im}$ , defined as  $Z/\sigma$ , increase at low frequencies and decrease at high frequencies (Figure S10). A frequency of 5 Hz maximized both signal intensity and signal-to-noise ratios.

For each concentration of the HSA analyte, three independent devices were used to perform five replicate measurements (Figure 4a). The coefficients of variation (COVs) ranged from 2.9 to 15%, commensurate with existing FDA-approved bioanalytical methods.<sup>46</sup> These COV values include the idiosyncrasies associated with fabrication at the hands of two experimentalists. In the future, print manufacturing could further lower device COVs. Calculated LOQs and LODs ( $10\sigma$  and  $3\sigma$ , where  $\sigma$  is the standard deviation of the blank)<sup>47</sup> are 1.0 and 0.13 nM, respectively, for HSA detection by these devices. In practice, the lowest consistently measurable HSA concentration was 5.0 nM (Figure 3a,b), which is lower than the limit of detection (7 mg/mL, 105 nM) obtained by HemoCue Albumin 201 Analyzer, a point-of-care system that quantifies albumin.<sup>48</sup>

At the highest protein concentrations examined here, gHSA consistently provided higher levels of impedance than HSA, despite both analytes exhibiting similar apparent binding affinities for  $\alpha$ HSA. At lower concentrations, impedance levels for the two analytes did not

markedly vary. This behavior was observed in samples prepared both in synthetic urine and in buffer (Figure 4b). Bohli reported a different device configuration applying an immunosensor to detect glycosylated HSA. This device results in decreased impedance, an effect opposite to our device, which the authors attribute to the electric charge differences of HSA and gHSA.<sup>49</sup>

HSA binding to the PEDOT surface in our device increases the measured impedance (Figure 3). This observation is consistent with a sensing mechanism in which electrolyte-filled channels within the PEDOT film become blocked by immobilized HSA. Channel blocking would be expected to increase the ionic resistance, and hence  $Z_{re}$ , while also increasing  $Z_{im}$ . In equation 1,  $Z_{im}$  is the imaginary impedance,  $\omega$  is the frequency of the alternating current, and  $C$  is the current amplitude.

$$Z_{im} = (\omega C)^{-1} \quad \text{Eqn 1}$$

In this mechanism,  $C$  decreases as water ( $\epsilon = 79$ ) within channels is displaced by bound protein with a range of hydrophobic and hydrophilic functionalities ( $\epsilon \approx 4-20$ ). In previous reports, we have proposed this mechanism to account for the resistance increase induced by HSA binding at phage-PEDOT composite films.<sup>50</sup> Glycation presents additional steric bulk, further impeding such ion transport and decreasing  $Z_{re}$  and  $Z_{im}$ . Collectively, the results support the proposed impedance-based sensing mechanism.

Six negative controls defined the biosensor and individual component responses to non-specific binding (Figure 4c). First, non-specific binding examined biosensor response to bovine serum albumin (BSA, a close homolog of HSA), a mixture of proteins from *E. coli* lysates, and an unrelated, high pI protein, phi29 DNA polymerase. Next, two different electrodes investigated the individual components of the biosensors as follows: a copper(II)-free PEDOT-IDA electrode evaluated non-specific binding of  $\alpha$ HSA and HSA to PEDOT-IDA, and an electrode without  $\alpha$ HSA examined non-specific binding of HSA to the PEDOT-Cu(II) complex. These controls had low signal-to-noise ratios, and generated impedance signals <10% of the positive controls.

The  $\alpha$ HSA electrode recognizes both HSA and gHSA equally well, but sandwich capture of gHSA allows discrimination of the two proteins. In this scheme, the boronic acid, conjugated to the DHFR reporter, forms covalent bonds with vicinal diols present on the glycosylated protein (Figure 2). The single-cysteine variant of DHFR used here was expressed in *E. coli* to avoid glycosylation, thus abrogating problems associated with self-dimerization and aggregation. Guided by a previous mutagenesis study,<sup>51</sup> we examined numerous mutant DHFR candidates and the variant reported here (N37C/C85A/C152S) exhibits no loss of activity compared to wild-type DHFR (Figure S14). The DHFR variant was labeled using a thiol-ene click reaction between the C37 thiol of DHFR and the alkene of 3-acrylamidophenylboronic acid. This step is described in detail in the Experimental Section.<sup>52</sup>

Binding of boronic acid-labeled DHFR to gHSA was detected by SWV measurements. The tetrahydrofolic acid produced through enzymatic catalysis is oxidized by the  $\alpha$ HSA electrode, generating a peak potential ( $E_p$ ) near +0.3 V versus MSE. The potential was scanned in PBS (pH 7.4) from  $-0.6$  to  $-0.8$  V with a step potential of 5 mV, an amplitude of 25 mV, and a frequency of 20 Hz. The obtained total current peak is proportional to the concentration of gHSA in the range of 1 to 1000 nM (Figure 5a). The corresponding calibration plot of the SWV response vs. gHSA concentration presents a logarithmic regression (Figure 5b). The lowest measurable gHSA concentration by the proposed biosensor is 1 nM, which is lower than the limit of detection obtained by the Lucica GA-L assay ( $7.9 \mu\text{M}$ ).<sup>53</sup>

HSA glycation ratios can be determined with this device. Mixtures of gHSA and its nonglycated counterpart (nHSA) were prepared such that the total gHSA+nHSA concentration was fixed at 500 nM. A significant increase in the current response with increasing gHSA ratios was observed in the range from 5 to 80% (Figure 5c). HSA obtained from recombinant expression in bacteria (rHSA), and BSA were used to evaluate non-specific binding by boronic acid labeled-DHFR in PBS and synthetic urine (Figure 5d). These controls generated a low signal of <8% the total current obtained from gHSA at the same concentrations.

## Conclusions

In summary, this report focuses on development of key elements for robust sensor fabrication. The reported sensors exhibit exceptional reproducibility, within tolerances for FDA-approved medical diagnostics. Sensor-to-sensor reproducibility is very high, despite the lack of sophisticated manufacturing techniques. COVs of 1.4–15% were obtained across the 1–1000 nM HSA concentration range. The biosensor utilizes a boronate-tagged DHFR enzyme for SWV signal amplification, which allowed gHSA to be discriminated at proportions of total HSA as low as 5%. Our design is readily amenable to large-scale manufacture of both the polymer electrode, and the protein-based sensing components. The modularity of our design lends itself to rapid development of alternative sensors with different specificities, which can be achieved through substitution of  $\alpha$ HSA with other His<sub>6</sub>-tagged ligands. Further development could establish sensors for point-of-care, at-home, or lab-based gHSA monitoring.

## Experimental Section

### General Experimental Methods

Three different human serum albumins (HSAs) have been used in this work: i) A lyophilized powder, fatty acid free, globulin free HSA with no carbohydrate content with a purity of >99.0% (Sigma-Millipore), ii) A lyophilized powder, *in vitro* glycated human serum albumin with 3 mol hexose (as fructosamine) per mol albumin (Sigma-Millipore), and iii) a recombinant human serum albumin from recombinant *Saccharomyces cerevisiae* fermentation, manufactured without the use of animal- or human-derived materials (Novozymes). The synthetic urine was Surine™ Negative Urine Control pH 6.9 (Sigma-

Millipore), a non-biological mixture commonly used as a negative reference standard for laboratory urine tests.

High resolution mass spectra (HRMS) were obtained by electrospray ionization (ESI) on a Waters (Micromass) LCT Premier equipped with a time-of-flight (TOF) mass analyzer. Proton ( $^1\text{H}$ , 500 MHz) and carbon ( $^{13}\text{C}$ , 125 MHz) nuclear magnetic resonance (NMR) spectra were obtained on a Bruker instrument equipped with a switchable BBFO probe. NMR samples were prepared in  $\text{CDCl}_3$  and  $\text{DMSO}-d_6$  and residual protonated solvent was used as an internal chemical shift standard.  $^1\text{H}$  and  $^{13}\text{C}$  assignments were determined using HSQC and 10 Hz optimized HMBC 2D-NMR analyses. Fourier-transform infrared (FTIR) spectra were obtained as neat samples on a Jasco 4700 attenuated total reflectance instrument using a diamond-coated zinc selenide sample accessory. Flash chromatography was carried out on silica gel 60 according to the procedure of Still *et al.*<sup>54</sup> Analytical thin layer chromatography (tlc) was conducted on aluminium-backed 2 mm thick silica gel 60 GF254 and chromatograms were visualized under a UV lamp (254 and 365 nm), or by chemical staining with ceric ammonium molybdate (Hanessian's stain) or  $\text{KMnO}_4$ .

### Synthesis of EDOT-pIDA

Chloromethyl EDOT (**1**).<sup>55</sup> 3,4-Dimethoxythiophene (1.30 g, 9.02 mmol),  $\alpha$ -chlorohydrin (3.02 mL, 36.1 mmol) and  $\text{TsOH}\cdot\text{H}_2\text{O}$  (343 mg, 1.80 mmol) were combined in a flame-dried 250 mL round-bottomed flask under nitrogen, then toluene (36 mL) was added, forming a two-phase heterogeneous mixture. The flask was fitted with a distillation head, and the reaction mixture was heated to 145 °C with stirring under  $\text{N}_2$  atmosphere. After 30 min, approx. 10 mL of distillate had collected in the receiving bulb, at which point the temperature was reduced to 125 °C. Reaction progress was monitored by TLC (1:1 hexanes/ $\text{CH}_2\text{Cl}_2$ ); complete conversion of the starting material (*rf*0.26) to product (*rf*0.52) was observed after 2.5 h. The black-colored reaction mixture was concentrated at 80 °C and 10 Torr on a rotary evaporator, and the crude was purified by flash chromatography (1:1 hexanes/ $\text{CH}_2\text{Cl}_2$ ) yielding 967 mg (56%) of **1** as a colorless liquid.  $^1\text{H}$  NMR (500 MHz,  $\text{CDCl}_3$ , 25 °C)  $\delta$  3.67 (1 H, dd,  $J$  11.6, 7.4 Hz,  $\text{CH}_2\text{Cl}$ ), 3.73 (1 H, dd,  $J$  11.6, 5.1 Hz,  $\text{CH}_2\text{Cl}$ ), 4.16 (1 H, dd,  $J$  11.8, 6.3 Hz,  $\text{CH}_2\text{O}$ ), 4.28 (1 H, dd,  $J$  11.8, 2.3 Hz,  $\text{CH}_2\text{O}$ ), 4.38 (1 H, dddd,  $J$  7.4, 6.3, 5.1, 2.3 Hz,  $\text{CH}_2\text{CHCH}_2$ ), 6.37 (1 H, d,  $J$  3.7 Hz,  $\text{SCH}$ ), 6.38 (1 H, d,  $J$  3.7 Hz,  $\text{SCH}$ ).  $^{13}\text{C}$  NMR (125 MHz,  $\text{CDCl}_3$ , 25 °C)  $\delta$  41.5 ( $\text{CH}_2\text{Cl}$ ), 65.7 ( $\text{CH}_2\text{O}$ ), 73.0 ( $\text{CH}_2\text{CHCH}_2$ ), 100.27, 100.29 (2 C,  $\text{CHSCCH}$ ), 140.8, 141.3 (2 C,  $=\text{C}-\text{C}=\text{C}$ ). IR  $\nu$  754.2, 848.1, 920.2, 947.7, 1010.8, 1062.3, 1181.5, 1375.3, 1426.6, 1478.9  $\text{cm}^{-1}$ . HRMS calcd for  $\text{C}_7\text{H}_8\text{ClO}_2\text{S}$  ( $\text{M}+\text{H}$ )<sup>+</sup> *m/z* 190.9928, found 190.9924.

Azidomethyl EDOT (**2**).<sup>56</sup> A solution of **1** (600 mg, 3.15 mmol) and sodium azide (409 mg, 6.29 mmol) in anhydrous DMF (10 mL) was heated to 120 °C on an oil bath under  $\text{N}_2$  atmosphere. Reaction progress was monitored by TLC (1:1 hexanes/ $\text{CH}_2\text{Cl}_2$ ); complete conversion of the starting material (*rf*0.52) to product (*rf*0.34) was observed after 1 h. The clear, yellow-colored reaction mixture was diluted with distilled water (90 mL), and the resulting cloudy white mixture was extracted with  $\text{Et}_2\text{O}$  ( $3 \times 25$  mL). The combined organic phases were dried over anhydrous  $\text{MgSO}_4$ , filtered and concentrated at 40 °C and 10 Torr on a rotary evaporator. The crude product was purified by flash chromatography (1:1



hexanes/CH<sub>2</sub>Cl<sub>2</sub>) yielding 601 mg (97%) of **2** as a colorless liquid (601 mg, 97%). <sup>1</sup>H NMR (500 MHz, CDCl<sub>3</sub>, 25 °C) δ 3.50 (1 H, dd, *J* 13.1, 5.2 Hz, CH<sub>2</sub>N<sub>3</sub>), 3.58 (1 H, dd, *J* 13.1, 6.1 Hz, CH<sub>2</sub>N<sub>3</sub>), 4.06 (1 H, dd, *J* 11.7, 6.9 Hz, CH<sub>2</sub>O), 4.20 (1 H, dd, *J* 11.7, 2.3 Hz, CH<sub>2</sub>O), 4.32 (1 H, dddd, *J* 6.9, 6.1, 5.2, 2.3 Hz, CH<sub>2</sub>CHCH<sub>2</sub>), 6.36 (1 H, d, *J* 3.7 Hz, SCH), 6.39 (1 H, d, *J* 3.7 Hz, SCH). <sup>13</sup>C NMR (125 MHz, CDCl<sub>3</sub>, 25 °C) δ 50.7 (CH<sub>2</sub>N<sub>3</sub>), 65.9 (CH<sub>2</sub>O), 72.6 (CH<sub>2</sub>CHCH<sub>2</sub>), 100.2, 100.4 (2 C, CHSCH), 140.8, 141.2 (2 C, =C=C=). IR ν 758.9, 856.1, 912.4, 928.1, 1020.4, 1081.8, 1181.9, 1253.3, 1376.9, 1480.3, 2095.8 cm<sup>-1</sup>. HRMS calcd for C<sub>7</sub>H<sub>8</sub>N<sub>3</sub>O<sub>2</sub>S (M+H)<sup>+</sup> *m/z* 198.0332, found 198.0327.

Nitrilotriacetic acid anhydride (**3**).<sup>57</sup> Pyridine (274 μL, 3.40 mmol) and Ac<sub>2</sub>O (3.09 mL, 32.7 mmol) were added to a suspension of nitrilotriacetic acid (NTA, 5.00 g, 26.2 mmol) in anhydrous DMF (10 mL) and the mixture was heated to 45 °C with stirring for 24 h under N<sub>2</sub> atmosphere. During this time the white suspension slowly transformed into a clear, yellow, homogenous solution. The reaction mixture was evaporated at 65 °C at 4 Torr on a rotary evaporator, yielding a viscous orange oil. The residue was dissolved in anhydrous DMF (20 mL), evaporated a second time, then dried at 10<sup>-3</sup> Torr for 48 h to yield a yellow chalky solid. The solid was dissolved in THF (25 mL) and the solution was added to stirring EtOAc (250 mL) at rt. The resulting white suspension was filtered on a Büchner funnel, and the solid was dried at 10<sup>-3</sup> Torr for 24 h, yielding 3.10 g (67%) of **3** as a brilliant white chalky solid. The product contained approx. 5% unreacted NTA. <sup>1</sup>H NMR (500 MHz, DMSO-*d*<sub>6</sub>, 50 °C) δ 3.46 (2 H, s, CH<sub>2</sub>CO<sub>2</sub>H), 3.82 (4 H, s, CH<sub>2</sub>NCH<sub>2</sub>), 12.69 (1 H, br s, CO<sub>2</sub>H). <sup>13</sup>C NMR (125 MHz, DMSO-*d*<sub>6</sub>, 50 °C) δ 51.5 (2 C, CH<sub>2</sub>NCH<sub>2</sub>), 54.3 (CH<sub>2</sub>CO<sub>2</sub>H), 165.7 (2 C, O=C-O-C=O), 171.7 (CO<sub>2</sub>H). IR ν 550, 606, 642, 700, 748, 837, 881, 931, 951, 995, 1005, 1099, 1118, 1130, 1209, 1232, 1255, 1271, 1296, 1323, 1360, 1430, 1447, 1715, 1776, 1820, 2527, 2608, 2736, 2952 cm<sup>-1</sup>. HRMS calculated for C<sub>7</sub>H<sub>11</sub>NNaO<sub>6</sub> (M+CH<sub>3</sub>OH+Na)<sup>+</sup> *m/z* 228.0484, found 228.0486.

EDOT-pIDA (**4**). Bu<sub>3</sub>P (4.68 mL, 19.0 mmol) was added via cannula to a solution of **2** (3.4 g, 17.2 mmol) in anhydrous THF (30 mL) at 0 °C under N<sub>2</sub> atmosphere, then the mixture was warmed to rt. A vigorous exothermic reaction occurred with significant gas evolution lasting approx. 2 min. During this time a pronounced color change was observed, beginning with a clear yellow solution, which then turns pink/red, and then finally bright orange. Then, a suspension of **3** (3.0 g, 17.2 mmol) in anhydrous THF (30 mL) was transferred to the reaction mixture via cannula under N<sub>2</sub> atmosphere. Upon contact with the reaction mixture, the white suspension immediately dissolved, resulting in a second color change from orange to yellow. No exothermic behavior was observed during this part. The reaction mixture was heated at 65 °C under reflux in N<sub>2</sub> atmosphere for 21 h, after which time the product was clearly visible by TLC analysis (2:1 CHCl<sub>3</sub>/MeOH, *r*<sub>f</sub> 0.33). The reaction mixture was concentrated at 40 °C at 150 Torr, and the residue was dried at 10<sup>-3</sup> Torr for 16 h. The crude was purified twice by flash chromatography (99:1:1 → 80:19:1 CHCl<sub>3</sub>/MeOH/AcOH, then 90:9:1 → 14:80:1 PhMe/EtOAc/AcOH) yielding 4.73 g (84%) of **4** as a clear, colorless, viscous oil. <sup>1</sup>H NMR (500 MHz, CDCl<sub>3</sub>, 25 °C) δ 3.51 (2 H, s, CH<sub>2</sub>CONH), 3.74 (4 H, s, CH<sub>2</sub>NCH<sub>2</sub>), 3.91 (1 H, dd, *J* 13.7, 5.2 Hz, CH<sub>2</sub>NH), 3.99 (1 H, dd, *J* 11.8, 6.6 Hz, CH<sub>2</sub>O), 4.18 (1 H, dd, *J* 11.8, 2.2 Hz, CH<sub>2</sub>O), 4.27 (1 H, dd, *J* 13.7, 7.4 Hz, CH<sub>2</sub>NH), 4.39 (1 H, dddd, *J* 7.4, 6.6, 5.2, 2.2 Hz, CH<sub>2</sub>CHCH<sub>2</sub>), 6.31 (1 H, d, *J* 3.7 Hz, SCH), 6.34 (1 H, d, *J* 3.7



Hz,  $SC\bar{H}$ ), 8.42 (1 H, br s,  $CON\bar{H}$ ).  $^{13}C$  NMR (125 MHz,  $CDCl_3$ , 25 °C)  $\delta$  38.9 ( $NH\bar{C}H_2$ ), 55.3 ( $\bar{C}H_2CONH$ ), 55.4 (2 C,  $\bar{C}H_2N\bar{C}H_2$ ), 66.5 ( $\bar{C}H_2O$ ), 71.0 ( $CH_2\bar{C}HCH_2$ ), 100.0, 100.3 (2 C,  $\bar{C}HS\bar{C}H$ ), 141.0, 141.3 (2 C,  $=\bar{C}-\bar{C}=\bar{C}$ ), 169.4 (2 C,  $O=\bar{C}-O-\bar{C}=\bar{O}$ ), 173.7 ( $\bar{C}ONH$ ). IR  $\nu$  606, 632, 700, 735, 767, 855, 861, 919, 1020, 1087, 1120, 1185, 1229, 1265, 1351, 1374, 1384, 1423, 1484, 1684, 1736, 2924, 3110  $cm^{-1}$ . HRMS calculated for  $C_{13}H_{14}N_2NaO_6S$  ( $M+Na$ )<sup>+</sup>  $m/z$  349.0470, found 349.0469.

### Biosensor fabrication and characterization

A 46×27×1 mm glass microscope slide was spin-coated with 0.5 M  $Fe(ClO_4)_3$  and 3% w/v nitrocellulose in 1:1 EtOH/Et<sub>2</sub>O (iron(III) perchlorate in collodion, 150  $\mu$ L) at 3500 rpm for 30 s (Figure 6a). Then, 62.7 mM EDOT and 3.3 mM EDOT-pIDA in *n*-BuOH (150  $\mu$ L) was spincoated directly onto the collodion/ $Fe^{(III)}$  film at 3500 rpm. The successful polymerization of the first PEDOT-pIDA layer can be confirmed visually through a color change of the film from yellow to dark blue. The next five consecutive layers were deposited by alternating between spin coats of 0.5 M  $Fe(ClO_4)_3$  in *n*-BuOH (150  $\mu$ L), then 62.7 mM EDOT and 3.3 mM EDOT-pIDA in *n*-BuOH (150  $\mu$ L). The slides were then placed in a polystyrene Petri dish with the PEDOT-pIDA face-up, and cured overnight at rt. The mature films were then washed under a stream of EtOH for 30 s, air-dried, then fitted with a PMMA 100  $\mu$ L capacity flow cell. The resulting device is bench stable, and no loss of performance was observed after storage for periods up to 30 days in air at rt. Hydrolysis of the IDA anhydride group is performed immediately prior to measurements.

Prior to measurements, the flow cell reservoir was first rinsed with 0.5 M aq. EDTA (20  $\mu$ L), then 4 M aq. NaOH (20  $\mu$ L), which causes hydrolysis of the anhydride protecting groups, then 10 mM PBS (pH 7.4, 100  $\mu$ L) (Figures 6b and S7). Each rinse solution was left to stand without agitation for 2 min, then carefully removed by pipette. The reservoir was then charged with 100 mM aq.  $CuSO_4$  (20  $\mu$ L), incubated for 30 min at rt without agitation, then the solution was removed by pipette. The reservoir was rinsed with 10 mM PBS (pH 7.4, 3 × 100  $\mu$ L), charged with 1  $\mu$ g·mL<sup>-1</sup>  $\alpha$ HSA in 10 mM PBS (pH 7.2, 20  $\mu$ L), and incubated for a further 30 min. The  $\alpha$ HSA solution was removed by pipette and the reservoir was rinsed with 10 mM PBS (pH 7.4, 3 × 100  $\mu$ L), providing a clean bioaffinity layer ready for electrochemical biosensing experiments. The surface morphology of the PEDOT-pIDA was examined by scanning electron microscopy (SEM) and atomic force microscopy (AFM) (Figures S5 and S6). The final thickness of collodion-PEDOT-pIDA layers was ~830 nm. The RMS surface roughness of a single layer of PEDOT-pIDA was 5 nm; RMS surface roughness of six layers of PEDOT-pIDA was 8 nm. Electrode surfaces were further characterized by contact angle analysis. A single drop (50  $\mu$ L) of distilled water was placed directly on the electrode surface and photographed with a DSLR camera (Nikon D60) equipped with a 60 mm macro lens (Figure S3). The water contact angle obtained for the nitrocellulose-coated glass surface was 15°. Contact angles increase with successive spin-coats of 95:5 PEDOT/PEDOT-pIDA; measured water contact angles were 50°, 65° and 70° for surfaces with two, four and six film layers, respectively. The increasing hydrophobicity of the surface is commensurate with increased coverage of the hydrophilic nitrocellulose by the film.<sup>45</sup> The formation of the ternary sensing complex on the PEDOT-IDA films were

characterized by impedance spectroscopy to illustrate changes in conductivity during the electrode assembly (Figure S8).

### Electrochemical impedance spectroscopy

Electrochemical impedance and square wave voltammetry were performed using a PalmSens3 controlled by PS-Trace 4.8 software (PalmSens BV, Houten, Netherlands). All electrochemical data was processed on GNU Octave, Igor Pro and OriginLab Pro 8 software. The impedance-frequency properties of the binding of  $\alpha$ HSA to HSA and gHSA were evaluated using a two-electrode system (Figure 7). The working electrode (PEDOT-Cu- $\alpha$ HSA bioaffinity layer) was connected to the input of a PalmSens3 potentiostat using a piece of copper tape fixed at its edge, and an alligator pin as electric contacts. The counter electrode (platinum foil) was connected to the output using an alligator pin and was inserted in the flow cell reservoir containing 100  $\mu$ L of the sample.

The frequency was scanned from 5 to 10,000 Hz with a 0.01 V alternating voltage. EIS was recorded and processed into an *impedance difference* ( $Z_{re}$ ), described as:  $Z = Z_{HSA} - Z_{buffer}$ , where  $Z_{HSA}$  and  $Z_{buffer}$  are the measured impedances before and after incubation with HSA for 5 min.

### Boronic acid modification of DHFR

The boronic acid-labeled DHFR used to discriminate gHSA from HSA was obtained via a thiol-ene reaction. A solution of 10 mM 3-acrylamidophenylboronic acid (3-APBA) and 20  $\mu$ M N37C/C85A/C152S DHFR in 10 mM PBS (pH 7.4, 500  $\mu$ L) was incubated on a shaker (5 rpm) at 4  $^{\circ}$ C for 10 h. The suspension was then transferred to a 5 kDa Amicon Ultra-0.5 mL centrifugal filter and centrifuged at 12,000 rpm and 4–5  $^{\circ}$ C for 10 min. The concentrate (15  $\mu$ L) was diluted with 10 mM PBS (pH 7.4, 485  $\mu$ L) and centrifuged a second time under the same conditions. Eight additional rounds of dilution/ultrafiltration were performed (total ultrafiltration steps = 10), which provides a high level of confidence that any unreacted 3-APBA remaining in the sample, if any, is negligible. The ultrafiltered and purified boronic acid labeled-DHFR was re-suspended in 10 mM PBS (pH 7.4), up to a final concentration of 5 nM. This stock was stored at 4  $^{\circ}$ C for later use in the biosensing experiments.

### Square wave voltammetry

The sensor was incubated with HSA and gHSA for 5 min before binding of boronate-labeled DHFR to surface-immobilized gHSA was assessed by SWV. A solution of 5 nM boronic acid-labeled DHFR (10  $\mu$ L) was added to the flow cell reservoir and incubated for 10 min, then washed with 10 mM PBS (pH 7.4,  $3 \times 100 \mu$ L). A solution of 5  $\mu$ M dihydrofolic acid and 5  $\mu$ M NADPH in 10 mM PBS (pH 7.4, 100  $\mu$ L) was then added to the reservoir (DHFR substrate and cofactor, respectively), and the SWV signal was measured immediately (Figures 2 and 5). The oxidation of tetrahydrofolic acid on PEDOT-IDA was detected at an applied potential of +0.3 V versus MSE. The potential was scanned in PBS (pH 7.4) from –0.6 to –0.8 V with a step potential of 5 mV, an amplitude of 25 mV, and a frequency of 20 Hz, and a baseline correction of the obtained voltammograms was performed using OriginLab Pro 8 software (Figure S11).

## Supplementary Material

Refer to Web version on PubMed Central for supplementary material.

## Acknowledgements

We gratefully acknowledge support from the National Cancer Institute of the NIH (1R33CA206955-01), the Chao Family Comprehensive Cancer Center of UCI, and the National Science Foundation, Chemistry Division through contract CHE-1306928. M.B.R. thanks the American Australian Association and the Dow Chemical Company for a Dow Chemical Company Fellowship. R.P.D. was supported by a training grant from the National Institute of Health (5T32CA009054-37). The authors thank Dr. Dmitry Fishman and the UCI Laser Spectroscopy Lab for use of the Jasco 4700 attenuated total reflectance instrument, Dr. Ming Tan from Wainamics for designing the flow cell, Prof. Phil Collins and laboratory (UCI, Physics) for use of their spin-coater, and Alana Ogata for her assistance with SEM and AFM characterization. We also thank Novozymes for the gift of recombinant HSA.

## References:

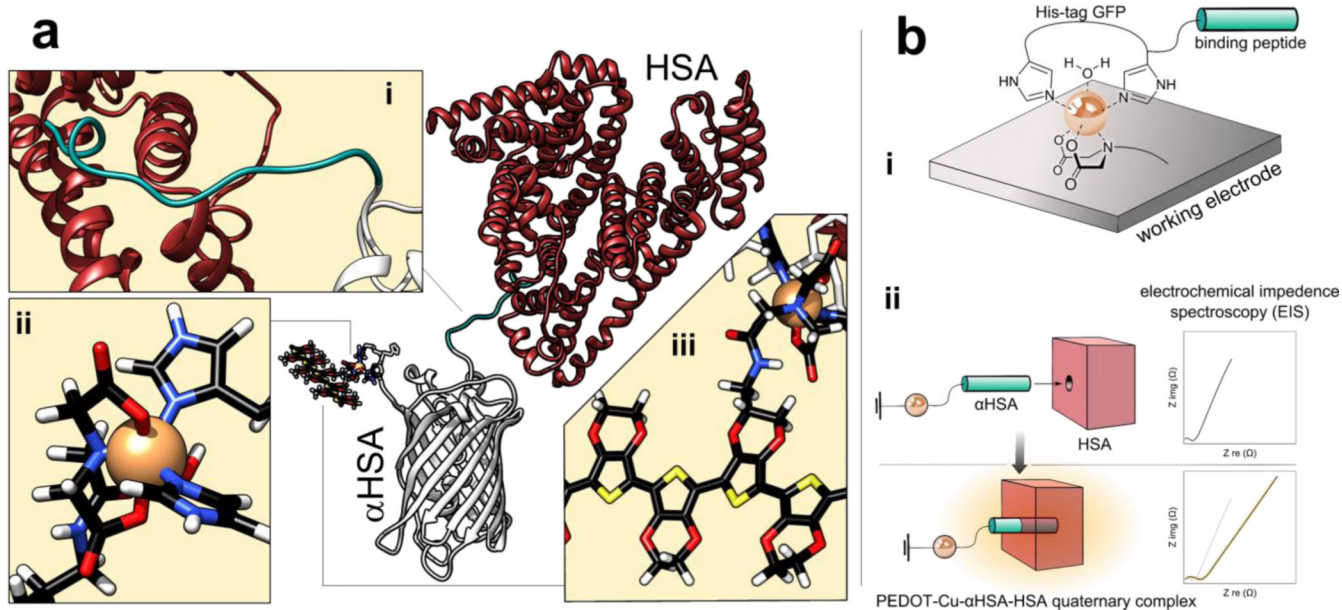
- (1). HSA as a biomarker in diagnostics and prognostics of solid tumors, rheumatoid arthritis, ischemia and severe acute graft-versus-host disease has been reviewed in: Fanali G; di Masi A; Trezza V; Marino M; Fasano M; Ascenzi P Human Serum Albumin: From Bench to Bedside Mol. Aspects Med 2012, 33, 209–290. [PubMed: 22230555]
- (2). Anguizola J; Matsuda R; Barnaby OS; Hoy KS; Wa C; DeBolt E; Koke M; Hage DS Review: Glycation of Human Serum Albumin Clin. Chim. Acta 2013, 425, 64–76. [PubMed: 23891854]
- (3). Jones CA; Francis ME; Eberhardt MS; Chavers B; Coresh J; Engelgau M; Kusek JW; Byrd-Holt D; Narayan KMV; Herman WH; Jones CP; Salive M; Agodoa LY Microalbuminuria in the US population: Third National Health and Nutrition Examination Survey Am. J. Kidney Dis 2002, 39, 445–459. [PubMed: 11877563]
- (4). Cravedi P; Ruggenti P; Remuzzi G Proteinuria Should Be Used as a Surrogate in CKD Nat. Rev. Nephrol 2012, 8, 301–306. [PubMed: 22391456]
- (5). Sarafidis PA; Bakris GL Microalbuminuria and Chronic Kidney Disease as Risk Factors for Cardiovascular Disease Nephrol. Dial. Transplant 2006, 21, 2366–2374. [PubMed: 16782993]
- (6). Koulouris S; Lekatsas I; Karabinos I; Ioannidis G; Katostaras T; Kranidis A; Triantafyllou K; Thalassinos N; Anthopoulos L Microalbuminuria: A Strong Predictor of 3Year Adverse Prognosis in Nondiabetic Patients With Acute Myocardial Infarction Am. Heart J 2005, 149, 840–845. [PubMed: 15894965]
- (7). Neelofar K; Ahmad J An Overview of In Vitro and In Vivo Glycation of Albumin: A Potential Disease Marker in Diabetes Mellitus Glycoconj. J 2017, 34, 575–584. [PubMed: 28812216]
- (8). Singh R; Barden A; Mori T; Beilin L Advanced Glycation End-Products: A Review Diabetologia 2001, 44, 129–146. [PubMed: 11270668]
- (9). Hodge JE; Rist CE The Amadori Rearrangement Under New Conditions and its Significance for Non-enzymatic Browning Reactions J. Am. Chem. Soc 1953, 75, 316–322.
- (10). Mendez DL; Jensen RA; McElroy LA; Pena JM; Esquerra RM The Effect of Non-enzymatic Glycation on the Unfolding of Human Serum Albumin Arch. Biochem. Biophys 2005, 444, 92–99. [PubMed: 16309624]
- (11). Roohk HV; Zaidi AR A Review of Glycated Albumin as an Intermediate Glycation Index for Controlling Diabetes J. Diabetes Sci. Technol. 2008, 2, 1114–1121. [PubMed: 19885300]
- (12). Ueda Y; Matsumoto H Recent Topics in Chemical and Clinical Research on Glycated Albumin J. Diabetes Sci. Technol 2015, 9, 177–182. [PubMed: 25614014]
- (13). Gan T; Liu X; Xu G Glycated Albumin Versus HbA1c in the Evaluation of Glycemic Control in Patients With Diabetes and CKD Kidney Int. Rep 2018, 3, 542–554. [PubMed: 29854962]
- (14). Wu W-C; Ma W-Y; Wei J-N; Yu T-Y; Lin M-S; Shih S-R; Hua C-H; Liao Y-J; Chuang L-M; Li H-Y Serum Glycated Albumin to Guide the Diagnosis of Diabetes Mellitus PLoS ONE 2016, 11, e0146780. [PubMed: 26765575]

- (15). Arasteh A; Farahi S; Habibi-Rezaei M; Moosavi-Movahedi AA Glycated Albumin: An Overview of the In Vitro Models of an In Vivo Potential Disease Marker *J. Diabetes Metab. Disord* 2014, 13:49. [PubMed: 24708663]
- (16). Kumar D; Banerjee D Methods of Albumin Estimation in Clinical Biochemistry: Past, Present, and Future *Clin. Chim. Acta* 2017, 469, 150–160. [PubMed: 28410855]
- (17). Aoyagi S; Iwata T; Miyasaka T; Sakai K Determination of Human Serum Albumin by Chemiluminescence Immunoassay with Luminol Using a Platinum-immobilized Flow-cell *Anal. Chim. Acta* 2001, 436, 103–108.
- (18). Choi S; Choi EY; Kim HS; Oh SW On-Site Quantification of Human Urinary Albumin by a Fluorescence Immunoassay *Clin. Chem* 2004, 50, 1052–1055. [PubMed: 15161719]
- (19). Comper WD; Jerums G; Osicka TM Differences in Urinary Albumin Detected by Four Immunoassays and High-performance Liquid Chromatography *Clin. Biochem* 2004, 37, 105–111. [PubMed: 14725940]
- (20). Marre M; Claudel JP; Ciret P; Luis N; Suarez L; Passa P Laser Immunonephelometry for Routine Quantification of Urinary Albumin Excretion *Clin. Chem* 1987, 33, 209–213. [PubMed: 3802503]
- (21). Thakkar H; Newman DJ; Holownia P; Davey CL; Wang C-C; Lloyd J; Craig AR; Price CP Development and Validation of a Particle-enhanced Turbidimetric Inhibition Assay for Urine Albumin on the Dade aca Analyzer *Clin. Chem* 1997, 43, 109–113. [PubMed: 8990231]
- (22). Watts GF; Bennett JE; Rowe DJ; Morris RW; Gatling W; Shaw KM; Polak A Assessment of Immunochemical Methods for Determining Low Concentrations of Albumin in Urine *Clin. Chem* 1986, 32, 1544–1548. [PubMed: 3089644]
- (23). Kohzuma T; Koga M Lucica® GA-L Glycated Albumin Assay Kit *Mol. Diagn. Ther* 2010, 14, 49–51. [PubMed: 20121290]
- (24). Ferri S; Kim S; Tsugawa W; Sode K Review of Fructosyl Amino Acid Oxidase Engineering Research: A Glimpse into the Future of Hemoglobin A1c Biosensing *J. Diabetes Sci. Technol* 2009, 3, 585–592. [PubMed: 20144298]
- (25). Abidin D; Liu L; Dou C; Datta A; Yuan C An Improved Enzymatic Assay for Glycated Serum Protein *Anal. Methods* 2013, 5, 2461–2469.
- (26). Paleari R; Bonetti G; Callà C; Carta M; Ceriotti F; Di Gaetano N; Ferri M; Guerra E; Lavalle G; Cascio CL; Martino FG; Montagnana M; Moretti M; Santini G; Scribano D; Testa R; Vero A; Mosca A Multicenter Evaluation of an Enzymatic Method for Glycated Albumin *Clin. Chim. Acta* 2017, 469, 81–86. [PubMed: 28365449]
- (27). Zheng D-J; Xu J; Su M-M; Sun Z-G; Jiao Q-C; Yang Y-S; Zhu H-L A Small, Steady, Rapid and Selective TICT Based Fluorescent HSA Sensor for Pre-clinical Diagnosis *Sens. Actuators B Chem* 2018, 271, 82–89.
- (28). Xu Y; Zhang M; Li B; Wang W; Wang B; Yang Y; Zhu H A Fluorescence Probe Acted on Site I Binding for Human Serum Albumin *Talanta* 2018, 185, 568–572. [PubMed: 29759242]
- (29). Singh P; Mittal LS; Kaur S; Kaur S; Bhargava G; Kumar S Self-assembled Small Molecule Based Fluorescent Detection of Serum Albumin Proteins: Clinical Detection and Cell Imaging *Sens. Actuators B Chem* 2018, 255, 478–489.
- (30). Samanta S; Halder S; Das G Twisted-Intramolecular-Charge-Transfer-Based Turn-On Fluorogenic Nanoprobe for Real-Time Detection of Serum Albumin in Physiological Conditions *Anal. Chem* 2018, 90, 7561–7568. [PubMed: 29792032]
- (31). Luo Z; Liu B; Zhu K; Huang Y; Pan C; Wang B; Wang L An Environment-sensitive Fluorescent Probe for Quantification of Human Serum Albumin: Design, Sensing Mechanism, and its Application in Clinical Diagnosis of Hypoalbuminemia *Dyes Pigm.* 2018, 152, 60–66.
- (32). Liu C; Yang W; Gao Q; Du J; Luo H; Liu Y; Yang C Differential Recognition and Quantification of HSA and BSA Based on Two Red-NIR Fluorescent Probes *J. Lumin* 2018, 197, 193–199.
- (33). Li P; Wang Y; Zhang S; Xu L; Wang G; Cui J An Ultrasensitive Rapid-response Fluorescent Probe for Highly Selective Detection of HSA Tetrahedron *Lett.* 2018, 59, 1390–1393.
- (34). Huang C; Ran G; Zhao Y; Wang C; Song Q Synthesis and Application of a Water-soluble Phosphorescent Iridium Complex as Turn-on Sensing Material for Human Serum Albumin *Dalton Trans.* 2018, 47, 2330–2336. [PubMed: 29367989]

- (35). Guo Y; Chen Y; Zhu X; Pan Z; Zhang X; Wang J; Fu N Self-assembled Nanosensor Based on Squaraine Dye for Specific Recognition and Detection of Human Serum Albumin Sens. Actuators B Chem 2018, 255, 977–985.
- (36). Groenendaal L; Jonas F; Freitag D; Pielartzik H; Reynolds JR Poly (3, 4-Ethylenedioxythiophene) and its Derivatives: Past, Present, and Future. Adv. Mater, 2000, 12, 481–494.
- (37). Huang PC; Shen MY; Yu HH; Wei SC; Luo SC Surface Engineering of Phenylboronic Acid-Functionalized Poly (3, 4-ethylenedioxythiophene) for Fast Responsive and Sensitive Glucose Monitoring. ACS Appl. Bio Mater 2018, 1, 160–167.
- (38). Hai W; Goda T; Takeuchi H; Yamaoka S; Horiguchi Y; Matsumoto A; Miyahara Y Specific Recognition of Human Influenza Virus With PEDOT Bearing Sialic Acid-terminated Trisaccharides. ACS Appl. Mater. interfaces 2017, 9, 14162–14170. [PubMed: 28379685]
- (39). Wei B; Liu J; Ouyang L; Kuo CC; Martin DC Significant Enhancement of PEDOT Thin Film Adhesion to Inorganic Solid Substrates With EDOT-acid. ACS Appl. Mater. Interfaces, 2015, 7, 15388–15394. [PubMed: 26052833]
- (40). Chen CH; Luo SC Tuning Surface Charge and Morphology for the Efficient Detection of Dopamine Under the Interferences of Uric Acid, Ascorbic Acid, and Protein Adsorption. ACS Appl. Mater. Interfaces, 2015, 7, 21931–21938. [PubMed: 26381224]
- (41). A thorough review of similar His-tag metal-affinity immobilizations of proteins onto electrodes for sensing applications appears in: Ley C; Holtmann D; Mangold K-M; Schrader J Immobilization of Histidine-tagged Proteins on Electrodes Colloid. Surf. B Biointerfaces 2011, 88, 539–551. [PubMed: 21840689]
- (42). Ogata AF; Edgar JM; Majumdar S; Briggs JS; Patterson SV; Tan MX; Kudlacek ST; Schneider CA; Weiss GA; Penner RM Virus-Enabled Biosensor for Human Serum Albumin Anal. Chem 2017, 89, 1373–1381. [PubMed: 27989106]
- (43). Mohan K; Donavan KC; Arter JA; Penner RM; Weiss GA Sub-nanomolar Detection of Prostate-Specific Membrane Antigen in Synthetic Urine by Synergistic, Dual-Ligand Phage J. Am. Chem. Soc 2013, 135, 7761–7767. [PubMed: 23614709]
- (44). Wang X; Xia N; Liu L Boronic Acid-Based Approach for Separation and Immobilization of Glycoproteins and its Application in Sensing Int. J. Mol. Sci 2013, 14, 20890–20912. [PubMed: 24141187]
- (45). Note: Higher loadings (10%, 20%, 50%, 100%) of PEDOT-pIDA were evaluated and showed a diminished electrode conductivity and device performances. Fewer than six cycles of polymerization resulted in devices with weakened specificities, possibly owing to non-specific interactions with exposed nitrocellulose.
- (46). US Food and Drug Administration. Guidance for Industry: Bioanalytical Method Validation Guidance for Industry Bioanalytical Method Validation. 2018, 1–22.
- (47). McNaught AD; Wilkinson A IUPAC, Compendium of Chemical Terminology. The Gold Book. 2nd ed. Blackwell Scientific Publications: Oxford 1997
- (48). USFDA 510(k) Substantial Equivalence Determination Decision Summary Assay and Instrument Combination Template. [https://www.accessdata.fda.gov/cdrh\\_docs/reviews/K053253.pdf](https://www.accessdata.fda.gov/cdrh_docs/reviews/K053253.pdf). Accessed 6 Dec 2018.
- (49). Bohli N; Meilhac O; Rondeau P; Gueffrache S; Mora L; Abdelghani A A Facile Route to Glycated Albumin Detection Talanta 2018, 184, 507–512. [PubMed: 29674076]
- (50). Yang L-MC; Diaz JE; McIntire TM; Weiss GA; Penner RM Direct Electrical Transduction of Antibody Binding to a Covalent Virus Layer Using Electrochemical Impedance Anal. Chem 2008, 80, 5695–5705. [PubMed: 18590279]
- (51). Antikainen NM; Smiley RD; Benkovic SJ; Hammes GG Conformation Coupled Enzyme Catalysis: Single-molecule and Transient Kinetics Investigation of Dihydrofolate Reductase Biochemistry 2005, 44, 16835–16843. [PubMed: 16363797]
- (52). Nair DP; Podgórski M; Chatani S; Gong T; Xi W; Fenoli CR; Bowman CN The Thiol-Michael Addition Click Reaction: A Powerful and Widely Used Tool in Materials Chemistry Chem. Mater 2014, 26, 724–744.

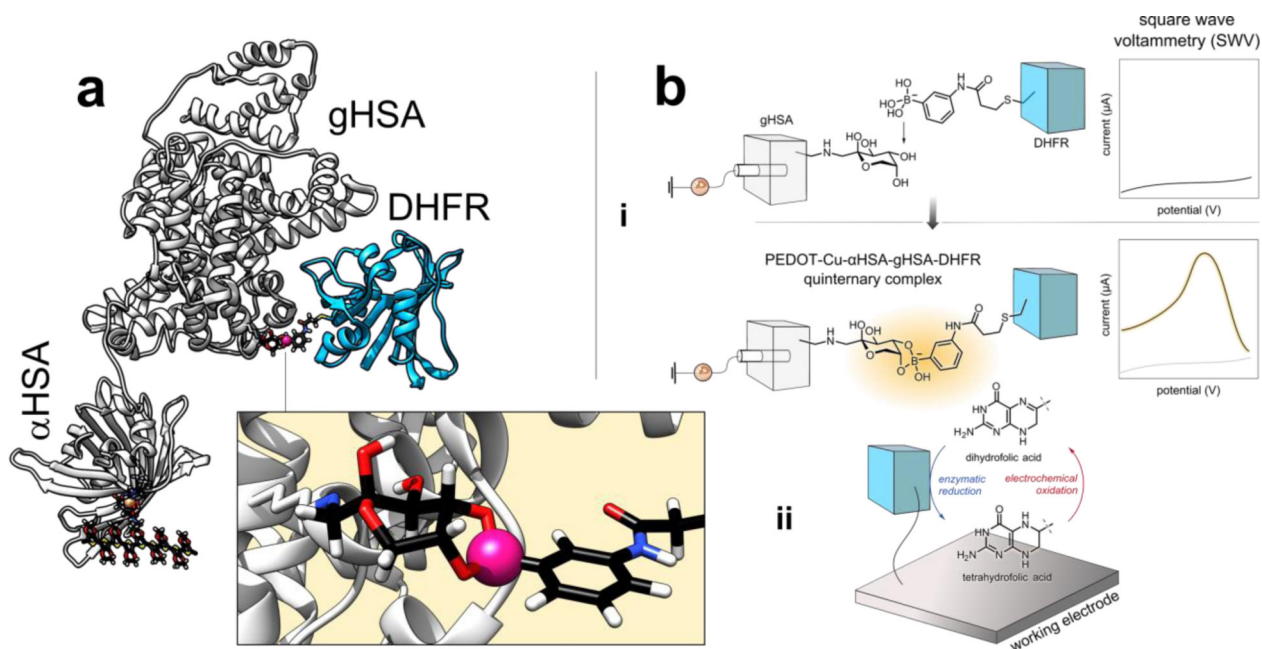
- (53). USFDA 510(k) Substantial Equivalence Determination Decision Summary Assay Only Template. [https://www.accessdata.fda.gov/cdrh\\_docs/reviews/K170147.pdf](https://www.accessdata.fda.gov/cdrh_docs/reviews/K170147.pdf). Accessed 6 Dec 2018.
- (54). Still WC; Kahn M; Mitra A Rapid Chromatographic Technique for Preparative Separations With Moderate Resolution J. Org. Chem 1978, 43, 2923–2925.
- (55). Segura JL; Gómez R; Reinold E; Bäuerle P Synthesis and Electropolymerization of a Perylenebisimide-functionalized 3,4-Ethylenedioxythiophene (EDOT) Derivative Org. Lett 2005, 7, 2345–2348. [PubMed: 15932194]
- (56). Bu H-B; Gotz G; Reinold E; Vogt A; Schmid S; Blanco R; Segura JL; Bauerle P “Click”-Modification of a Functionalized Poly(3,4-Ethylenedioxythiophene) (PEDOT) Soluble in Organic Solvents Chem. Commun 2008, 48, 2677–2679.
- (57). Rolleston RE, Merck & Co. Inc. Tc99m-Phenida, Radioscintigraphic Agent for Diagnosis of Hepatoniliary Disease USP 4,454,107, 1984, p 4.



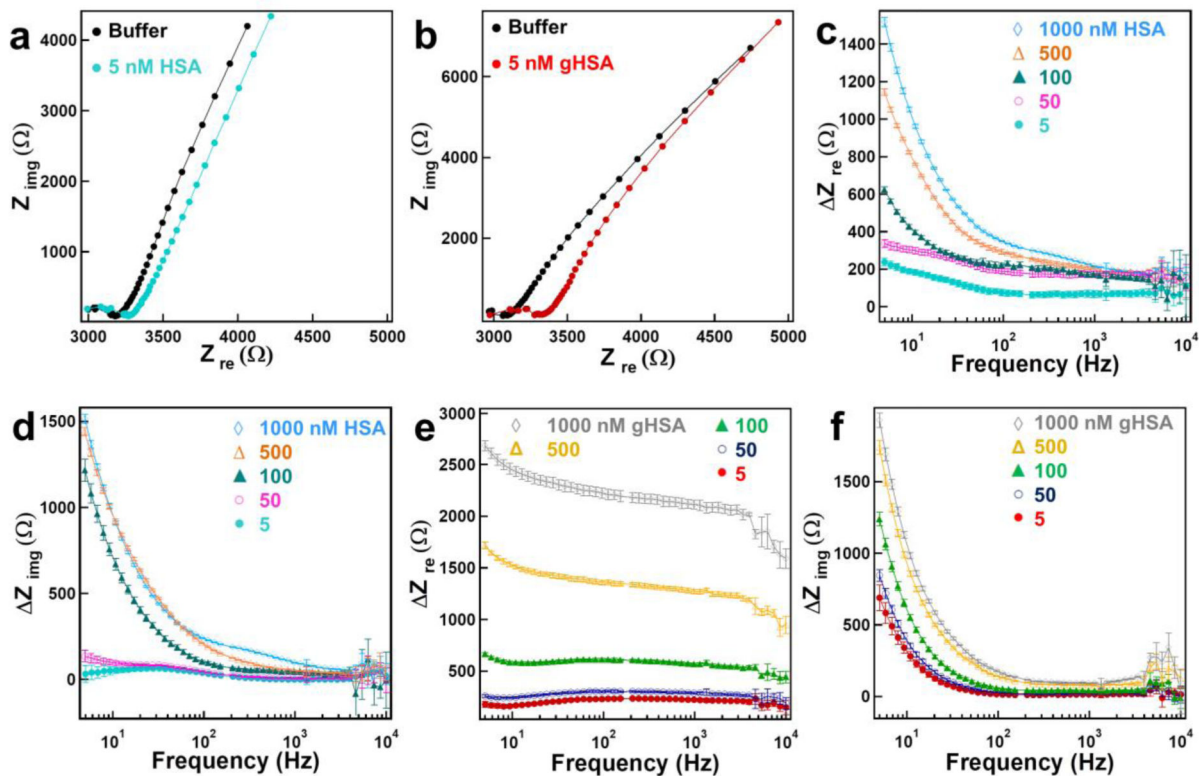


**Figure 1.** Schematic of the reported biosensor. (a) (i) HSA-binding peptide of  $\alpha$ HSA is depicted as a green-colored random coil. (ii) Immobilized Cu(II)-His<sub>6</sub> complex. Coordinating IDA and His ligands are depicted as rounded sticks bound to copper(II) (orange). (iii) Co-polymer of EDOT and EDOT-IDA. (b) Simplified illustration of the sensor, including (i) device architecture, and (ii) EIS sensing.



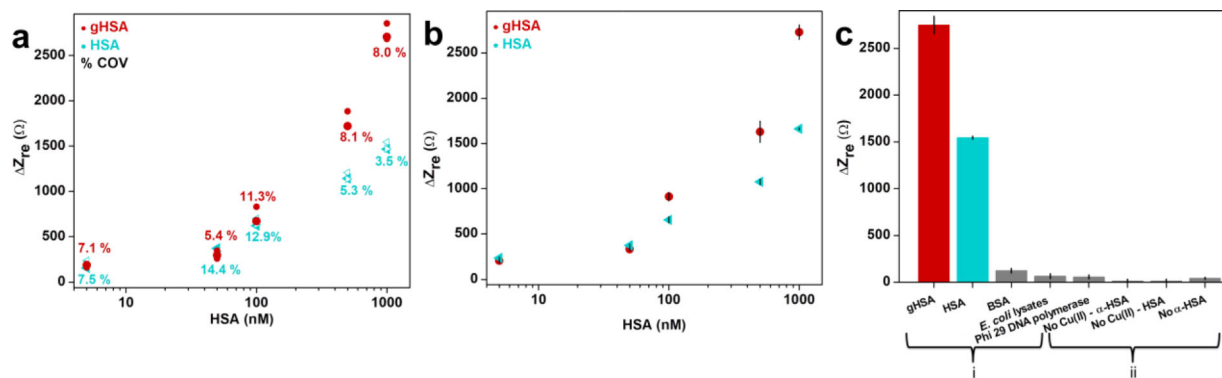


**Figure 2.** Schematic representation of gHSA quantification. (a). DHFR (blue ribbon) associates with surface carbohydrates on gHSA via its boronate affinity tag. The surface-exposed fructosamine residue and phenyl boronic ester (pink) are depicted as sticks. (b) (i) The gHSA-sensing complex is detected electrochemically via square-wave voltammetry (SWV) via (ii) redox cycling of dihydrofolic acid/tetrahydrofolic acid.



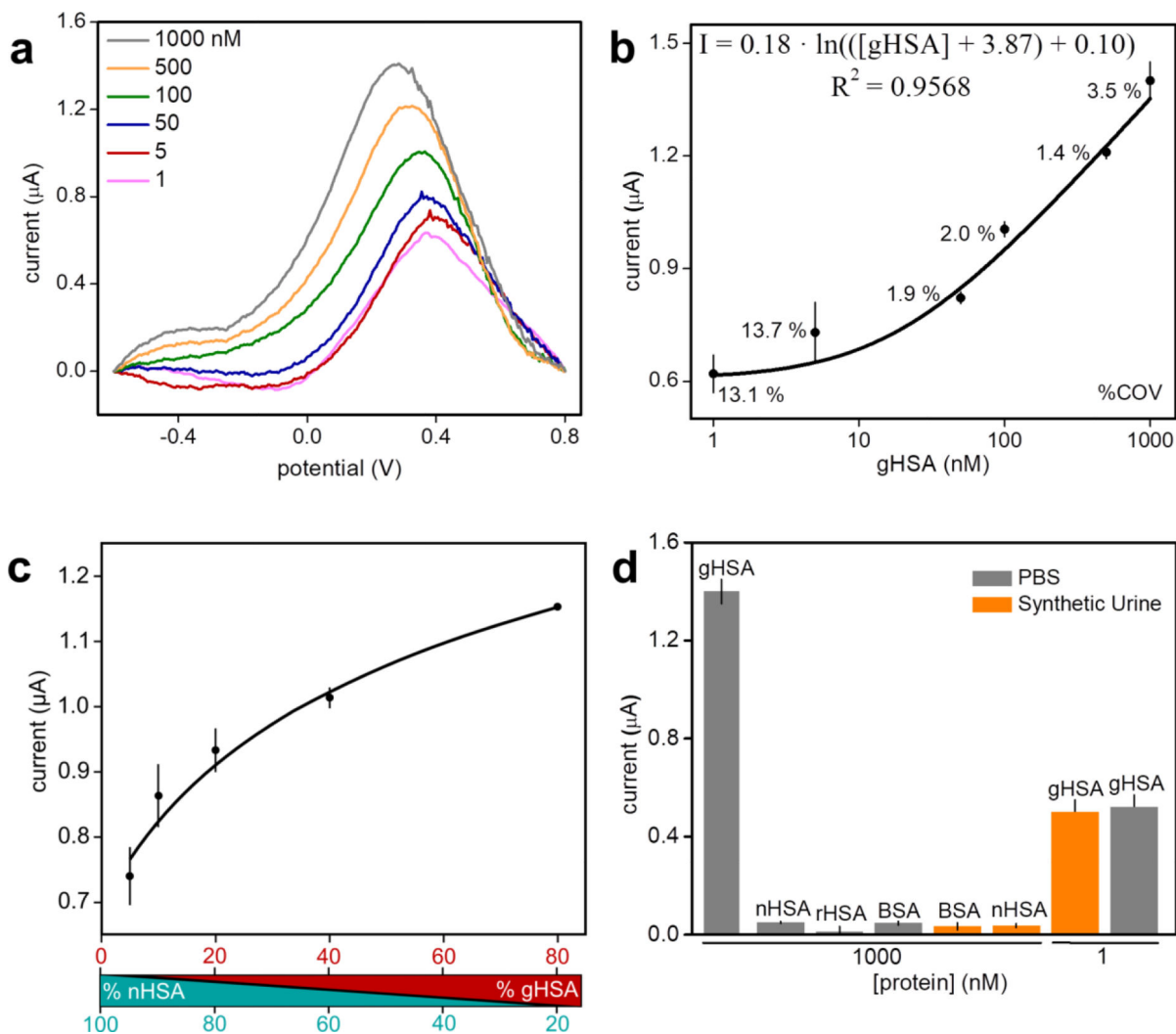
**Figure 3.**

EIS detection of HSA and gHSA. (a, b) Nyquist plots for PEDOT-IDA biosensors in solutions of buffer (black) and 5 nM HSA (blue) or gHSA (red). (c-f)  $Z_{re}$  and  $Z_{im}$  plots versus frequency for PEDOT-IDA biosensors exposed to varying concentrations of HSA (c,d) and gHSA (e,f), where  $Z$  is defined as  $Z_{HSA} - Z_{buffer}$ . Error bars are defined as propagated error from the standard deviation,  $\pm 1\sigma$ , for five consecutive EIS measurements.

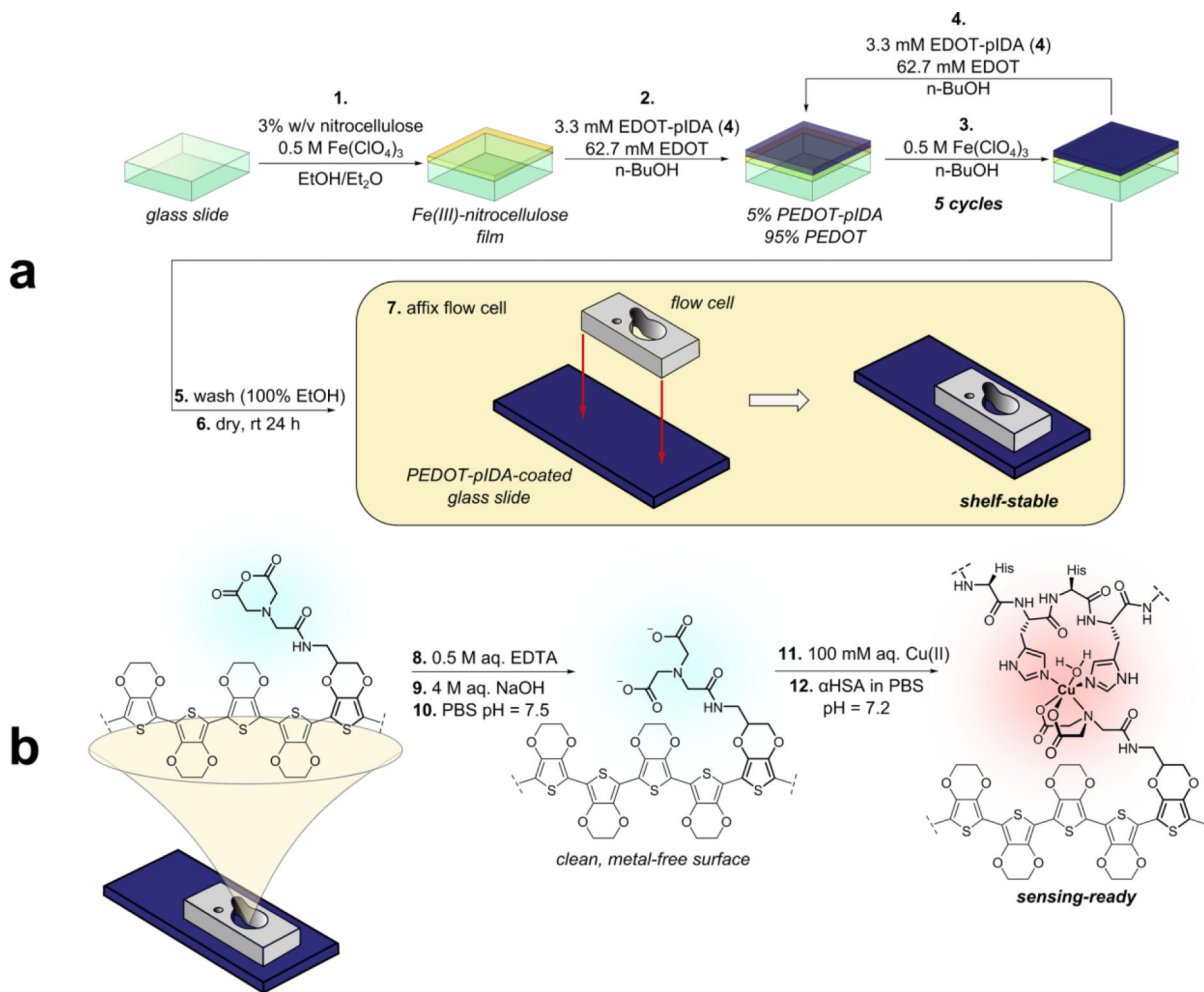


**Figure 4.**

Detection of HSA and gHSA by electrochemical impedance spectroscopy. Calibration plot of  $Z_{re}$  versus HSA concentrations for independent PEDOT-IDA biosensors exposed to the indicated concentrations of gHSA or HSA in (a) PBS (three independent devices for each concentration with 5 measurements each with the indicated % COVs) or (b) synthetic urine (one device for each concentration with 5 measurements each). Each data point represents the average obtained from five measurements on one device; error bars indicate standard deviations. (c) Control experiments confirm specific detection of gHSA and HSA, and demonstrate the necessity of each component in the quaternary sensing complex for device function. Proteins were tested at concentrations of 1000 nM.

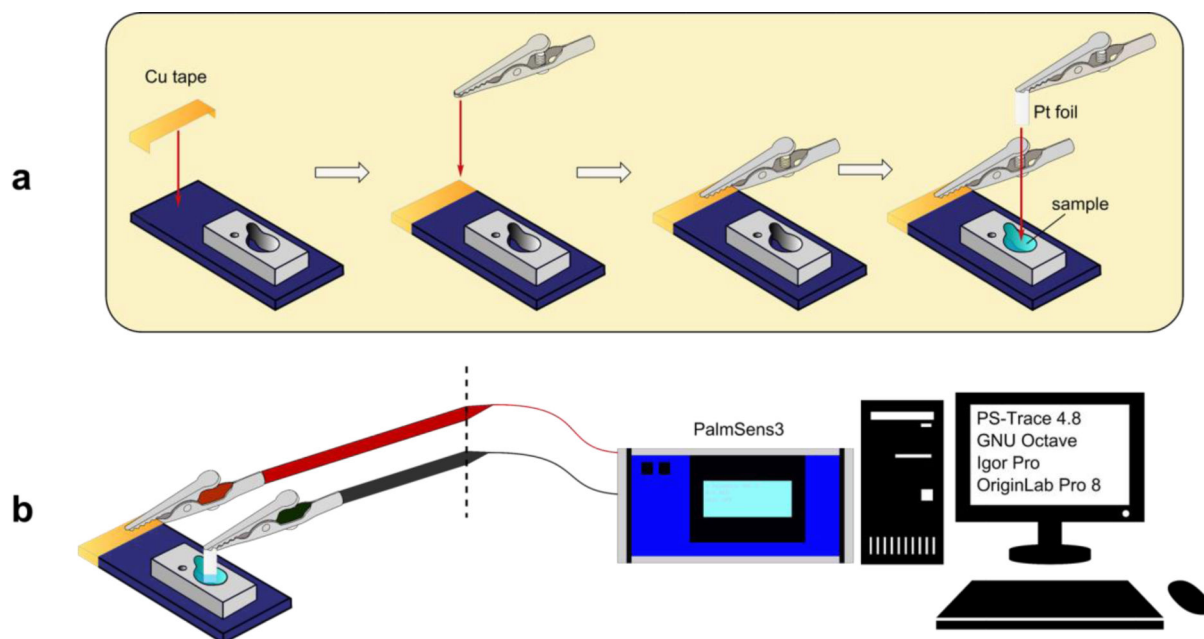


**Figure 5.** gHSA quantification. (a) Square wave voltammetry with the indicated gHSA concentrations. (b) Calibration plot of current versus gHSA concentration for 18 independent PEDOT-IDA biosensors exposed to the indicated concentrations of gHSA before incubation with boronic acid-labeled DHFR, NADPH and dihydrofolic acid. The percentages indicate COVs for three devices. The logarithmic equation represents the curve fit to the depicted data. (c) Current versus proportion of gHSA in gHSA+HSA mixtures after detection via SWV with boronic acid-labeled DHFR (three independent biosensors at each concentration, total [nHSA+gHSA] is 500 nM in all cases). (d) Control experiments verify specific binding of gHSA, non-glycated HSA (nHSA) isolated from healthy humans, recombinant HSA (rHSA), which also lacks glycation, and BSA to PEDOT-IDA biosensor and boronic acid-labeled DHFR in PBS (gray) and synthetic urine (orange).

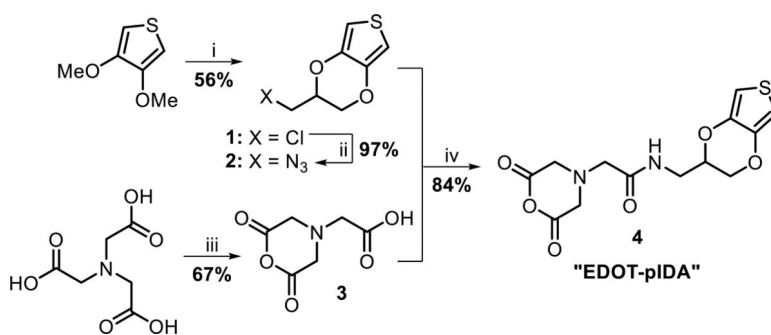


**Figure 6. Biosensor Fabrication.**

(a) Steps 1–6 of the procedure afford a shelf-stable electrode polymer with its IDA groups protected as anhydrides (PEDOT-pIDA). The film is highly stable in this configuration and can be stored in air at ambient temperatures for extended periods of time. The shelf life was tested up to 30 days without incurring any appreciable loss of device performance. (b) Only a small area of the PEDOT-pIDA film contained by the walls of the flow cell was further elaborated to an active sensor. The surface at the bottom of the flow cell is first washed, then its anhydride groups are hydrolyzed. The ternary sensing complex is then constructed by sequential treatment with aq.  $\text{CuSO}_4$ , then a buffered solution of the His<sub>6</sub>-tagged  $\alpha\text{HSA}$  in PBS.



**Figure 7.** Preparation of the biosensor for measurements. (a) Electrical contacts to the prepared devices are made with copper tape, platinum foil (as the counter electrode) and alligator pins. (b) Measurements were performed using a PalmSens3 analyzer controlled by PS-Trace 4.8. Data was processed with GNU Octave, Igor Pro, and OriginLab Pro 8.

**Scheme 1.**

*Reagents and conditions* i)  $\alpha$ -chlorohydrin, TsOH, PhMe, 145 °C, 30 min, then 125 °C, 2.5 h; ii) NaN<sub>3</sub>, DMF, 120 °C, 1 h; iii) Ac<sub>2</sub>O, Py., DMF, 45 °C, 24 h; iv) Bu<sub>3</sub>P, THF, 65 °C, 21 h.